Multi-Regional Optimal Power Flow Using Marine Predators Algorithm Considering Load and Generation Variability

RANIA A. SWIEF[1], **(Senior Member, IEEE), NADA MAMDOUH HASSAN**[1],
HANY M. HASANIEN[1], **(Senior Member, IEEE),**
ALMOATAZ YOUSSEF ABDELAZIZ[2], **(Senior Member, IEEE),**
AND MOHAMED Z. KAMH[1], **(Senior Member, IEEE)**
[1]Electrical Power and Machines Department, Faculty of Engineering, Ain Shams University, Cairo 11517, Egypt
[2]Faculty of Engineering and Technology, Future University in Egypt, Cairo 11835, Egypt

Corresponding author: Mohamed Z. Kamh (mohamed.zakaria@eng.asu.edu.eg)

ABSTRACT This paper introduces the application of a newly developed heuristic nature-inspired optimization technique, viz, tuned Marine Predator Algorithm (MPA), to solve the optimal power flow (OPF) problem of multi-regional systems. The paper proposes MPA parameters' tuning to enhance the algorithm performance. The paper takes into account the variability of different types of renewable energy resources (RERs) and loads. Two modeling approaches are presented: holistic (multi-regions are modeled as one large network) and inter-bounded (modeling the regional interfaces). The MPA is applied to the IEEE-48 bus connected system, and the results are compared with another well-established heuristic algorithm, namely the Genetic Algorithm (GA). The results demonstrate the validation, applicability and effectiveness of using the MPA for solving multi-region OPF problem considering renewable energy sources and load variability.

INDEX TERMS IEEE 48-Bus system, marine predator algorithm, multi-regional systems, optimal power flow, renewable energy resources.

I. INTRODUCTION

Resilience operation of modern power systems is becoming of increased importance due to the interconnection of several regions and the accelerated proliferation of non-dispatchable renewable energy sources and distributed generation. Albeit these new challenges, grid operators are mandated to achieve the most economical operations strategies as well as coordinating the generation in order to minimize the operation cost of the grid [1]. Typically, the electrical networks have some restrictions for the voltage of the buses, in addition to the power transmitted. These restrictions arise due to equipment rating, system stability and security [2].

Finding the resilient optimal safe operating condition of the power system is known as the security-constrained optimal power flow (OPF) problem. Mathematically, the OPF is a non-linear, non- convex optimization problem with an objective cost function subject to a set of equality and inequality constraints. OPF objective functions aim at minimizing one

or more of the following: fuel cost, emission cost, network losses, etc [3]. Control variables that are utilized in the OPF problem include generators scheduled voltage, generators dispatch level, transformer tap-settings, scheduled compensate reactive power, etc [4].

In multi-regional power systems, OPF variables include shared data from the neighboring connected areas, namely, magnitudes and angles of boundary voltages and interconnection line flows. Solving Inter-regional OPF can be done in two ways: using holistic method, or iteratively using the inter-bounded approach. In the holistic technique, the multi-regional network is counted as one large grid, while for the inter-bounded technique, the control variables of the interconnected borders between the areas are only considered [5], [6].

Several optimization approaches have been deployed to solve the OPF problem. These approaches are categorized into classical and artificial intelligence-based approaches. Classical optimization techniques include linear programming [7], non-linear programming [8], interior point method [9], quadratic programming [10], Newton-Raphson (NR) [11], and semi-definite method [12]. These techniques

are reported to (a) possibly get trapped in local minima instead of achieving the global optimum solution of the OPF problem, (b) be computationally demanding, and (c) the best solution is strongly affected by the initial guess of the problem [13], [14]. In an attempt to get over these drawbacks and difficulties, artificial intelligence-based optimization techniques are developed [15]. Artificial intelligence-based optimization mostly utilizes meta-heuristic techniques. These techniques are categorized into evolutionary-based, swarm-based, and physics-based strategies. Some of these techniques were used to solve the OPF problem, e.g., genetic algorithm (GA) [16], modified particle swarm optimization (PSO) [17], artificial bee colony (ABC) [18], grey wolf optimizer [19], flower pollination algorithm (FPA) [20], moth-flame optimization (MFO) [21], ant colony optimization (ACO) [22], gravitational search algorithm (GSA) [23], whale optimization algorithm (WOA) [24], [25], multi-objective dragonfly algorithm (MODA) [26], shuffled frog leaping algorithm (SFLA) [27], cuckoo Optimization Algorithm (COA) [28], Jaya optimizer [29], tree seed algorithm (TSA) [30], Sine-Cosine algorithm [31], and sunflower optimization (SFO) [32]. In [33], improved GA is applied to solve the OPF problem of a single area system by considering the presence of renewable energy resources and energy storage units. The PSO is implemented in [34] to decide the optimum hourly load flow with the incorporation of renewable distributed generation (DG) under various operating conditions in a single regional system. The Crow Search Algorithm (CSA) is used in [35] to solve OPF applied to the IEEE 30 bus system. In [36], an efficient evolutionary algorithm (EEA) was established to solve the OPF problem for IEEE 30, 118, and 300 bus. In [37], a teaching-learning-based optimization (TLBO) technique employing the Lévy mutation approach for optimal settings of OPF problem control variables was investigated. In [38], an algorithm based on the Shuffle Frog Leaping Algorithm (SFLA) was introduced in order to obtain the results for multi-objective OPF. A modified SLFA (MSLFA) technique was also presented to reduce the computational burden while improving the solution accuracy. The Salp swarm algorithm (SSA) is employed in [39] for solving different objective functions of OPF.

The Marine predator algorithm (MPA) is a newly developed heuristic nature-inspired optimization algorithm [40]. MPA mimics the dominant forage trend in ocean predators and the optimum conflict rate approach in the relationship between predator and prey in marine environments. MPA is an efficient meta-heuristic with many benefits, including the reduced number of variables configured, compact structure, noticeable convergence velocity, near-global approach, consistency, problem independence, and gradient-free nature [41]. The MPA has been implemented in [42] to precisely calculate the unidentified electrical nine variables of the triple-diode photovoltaic (TDPV) configuration of a PV module. Furthermore, the MPA is being used in the prediction of confirmed Covid-19 cases [43].

This paper proposes a novel application of the MPA to solve the highly non-linear and non-convex OPF problem for multi-regional networks, considering the variability of loads and renewable resources. In particular, the key contributions of this paper are as follows: (i) investigating the effect of different controlling parameters of MPA on the solver accuracy, (ii) modeling the OPF of multi-regional networks considering two different approaches (holistic and inter-bounded), and (c) considering the variability effect of loads and intermittent generation. The tuned MPA is applied to IEEE-48 bus connected network under various scenarios by using MATLAB program.

This paper is structured as follows. Section II illustrates the OPF objective functions and its constraints for multi-regional electric systems under two set-ups: holistic and inter-bounded approaches. Section III explains the MPA algorithm. Section IV describes the study system. Simulation results and analysis are detailed in sections V-VII. Conclusions and recommendations are presented in Section VIII.

II. PROBLEM FORMULATION

In this section, direct current (DC) OPF mathematical formulation is presented. In addition, modeling of the multi-regional OPF problem using the holistic and inter-bounded approaches is illustrated. Also, the renewables-based intermittent generation is considered as an integrated part of the OPF models well as the weekly variable load profile.

A. DC-OPF

DC-OPF is considered a simplified version of the OPF problem by ignoring the resistance of the transmission lines, hence linearizing the non-linear equations. Compared to AC-OPF, DC-OPF often decreases the calculation time. The DC-OPF governing equations are illustrated in equations (1)-(3) [44].

$$Min \sum_{u \in \Omega_G} f(P_u) \tag{1}$$

Subjected to,

$$h(P): \begin{cases} P_i - d_i = \sum_{j \in \Omega_i} \dfrac{\theta_i - \theta_j}{X_{ij}} & \forall i \in \{1, 2 \ldots N_b\} \\ \theta_{ref} = 0 \end{cases} \tag{2}$$

$$g(P): \begin{cases} \underline{P_u} \leq P_u \leq \overline{P_u} & \forall u \in \Omega_G \\ \dfrac{\theta_i - \theta_j}{X_{ij}} \leq \overline{PL}_{ij} & \forall ij \in \Omega_L \\ \underline{V_i} \leq V_i \leq \bar{V}_i & \forall i \in \Omega_L \end{cases} \tag{3}$$

where, θ is the angle of the bus voltage, $\underline{V}_i$ and $\bar{V}i$ are the minimum and maximum acceptable values of the bus voltage I, $P\bar{L}ij$ is the maximum flow allowed in branch ij (due to thermal limitations or other factors), P_i and d_i is the net generation and demand at the ith bus, Ω_G is the set of all the generating units in the grid, Ω_i is the set of all the generators connected to ith bus, Ω_L is the set of all the branches. $f(P_u)$ is the cost equation of the uth generator with dispatch P_u.

The latter two functions $h(x)$ and $g(x)$ are the equality and inequality constraints, respectively. Balances at nodal power flow and the adjustment for the voltage angle of the reference bus to zero are ensured by (2). Inequality (3) guarantees that the output power of generating unit u, the voltage at bus I, and the power flow in transmission line ij are within respective ranges.

B. HOLISTIC VERSUS INTER-BOUNDED OPF
The network of linked areas, as shown in Fig. 1, consists of individual regions connected by one or more transmission corridors. In the holistic method, the connected networks are considered as one large network, for which OPF is solved to find the control variables of both systems simultaneously. In the inter-bounded method, each region's OPF is solved separately while considering the inter-connected boundaries between the two areas separately [45]. It is obvious from the planning point of view, that changing or controlling more parameters in the system, in case of holistic, will lead to better improvement in the system performance. On the other hand, the time and effort will increase in controlling the whole system parameters. So, if the changes need fast action to be taken, the reliability coordinator between the regions will go to the inter-bounded solution for a fast optimum decision.. The study in this paper investigates the effect of both modeling options.
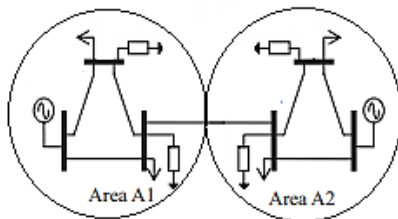

FIGURE 1. I Two-Area system.

C. RENEWABLES RESOURCES
In practice, the output of wind and solar renewable energy resources (RERs) is intermittent in nature. Thus, the generated energy from these sources is variable and non-dispatchable. Typical wind and solar daily output profiles are illustrated in Figs. 2 and 3, respectively [46]–[48]. The cost of both wind/solar energies is taken from the International Renewable Energy Agency (IRENA), the cost of solar energy is equal to 14.597 \$/MW and for wind energy, the cost is equal to 10 \$/MW [47].

III. MARINE PREDATOR ALGORITHM
The MPA is a metaheuristic (MH) algorithm that adopts the survival of the fittest strategy. In the MPA, both predator and prey are search agents, since the predator looks for the prey, which in turn looks for its food [40].

As all MH approaches based the foraging approach of animals, MPA relies on the stochastic strategy, in which it starts by discovering the search space and get random ranges of
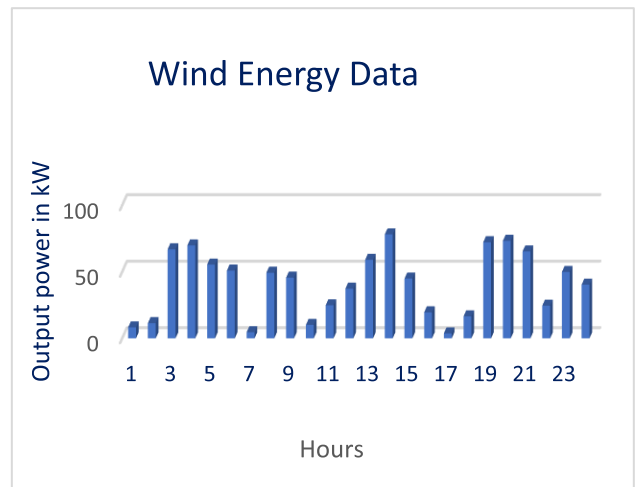
FIGURE 2. Wind profile for a day.
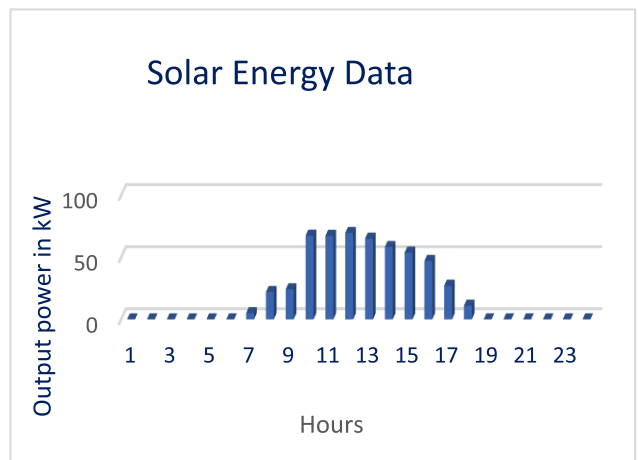
FIGURE 3. Solar profile for a day.

initial solutions. Afterwards, the solutions are tailored based on the algorithm's primary framework, where the next location (solution) will be based on the current location. Marine predators alter between two search strategies while searching for their prey, namely, Lévy and Brownian strategies, based on the prey availability. In areas with lower prey collection, the predators use a Lévy movement, while the Brownian movement is applied when there is abundance of prey [40].

The initial solutions are arbitrarily selected and the position updates are evaluated according to Eq. (4):

$$y_0 = y_{min} + rand * (y_{max} - y_{min}) \qquad (4)$$

where y_{max} and y_{min} are the design variable's upper and lower bound, respectively, and *rand* is a random vector ϵ [0,1].

In the MPA, there are two main matrices: The *Elite/Best matrix* (the fittest predators) and the Pray matrix, as depicted

in Eq. (5) and (6):

$$Elite = \begin{bmatrix} y_{11}^1 & y_{12}^1 & \cdots & y_{1d}^1 \\ y_{21}^1 & y_{22}^1 & \cdots & y_{2d}^1 \\ \cdots & \cdots & \cdots & \cdots \\ y_{n1}^1 & y_{n2}^1 & \cdots & y_{nd}^1 \end{bmatrix} \quad (5)$$

in which, $\overrightarrow{y^1}$ is a vector of the fittest predators that repeated n times to organize *Elite* matrix. The parameters n and d refer to the number and dimensions of the agents, accordingly. The *Elite* is updated subsequent to each iteration by substituting predators with better ones. The *Prey* matrix has the same dimensions as the *Elite* matrix, and is the basis for the predators to update their positions. The *Prey matrix* is represented as follows:

$$Prey = \begin{bmatrix} y_{11} & y_{12} & \cdots & y_{1d} \\ y_{21} & y_{22} & \cdots & y_{2d} \\ \cdots & \cdots & \cdots & \cdots \\ y_{n1} & y_{n2} & \cdots & y_{nd} \end{bmatrix} \quad (6)$$

in which, y_{ij} is the j-th dimension for i-th prey. For searching, the MPA imposes random variables and operators during the iterations to prevent the optimizer from getting trapped in local minima [40].

A. MPA PHASES

The MPA is based on imitating the whole life of the prey and predator. The speed ratio between the prey and the predator is the most significant control parameter of the MPA during the iterations. Based on the value of this parameter, the MPA is divided into three major phases, high-speed ratio in the first phase, unity ratio in the second phase, then sub-unity ratios in the last phase. For each defined phase, a specific number of iterations is specified. Details of each phase are presented in [40] and summarized in the following section.

1) FIRST PHASE: THE EXPLORATION STAGE

In the exploration phase, the prey is faster than the predator, i.e., speed ratio is greater than 10. This phase takes place in the first one-third of the iterations. In this stage, the fittest predators do not move at all, while the prey moves very rapidly to secure their food. This stage is represented mathematically by Eq. (7) and (8) [40]:

For $Iter < \frac{1}{3}Iter_{Max}$

$$\overrightarrow{stepsize_i} = \overrightarrow{R_B} \otimes \left(\overrightarrow{Elite_i} - \overrightarrow{R_B} \otimes \overrightarrow{prey_i} \right) \quad (7)$$

where, $i = 1, 2, 3, \ldots n$

$$\overrightarrow{prey_i} = \overrightarrow{prey_i} + P.\overrightarrow{R} \otimes \overrightarrow{stepsize_i} \quad (8)$$

where $\overrightarrow{R_B}$ is a normally distributed random vector representing the Brownian movement. The notation $\otimes$ marks out the vector multiplications, P is a constant equal to 0.5, and R constitutes a uniform random vector within [0,1]. *Iter* and *IterMax* are the current and maximum number of iterations, respectively.

2) SECOND PHASE: TRANSITION STAGE

In this stage, the predator and prey travel at nearly the same speed. In this phase, the prey (half of the population) is responsible for exploitation, and exploration is the responsibility of the predator. Eqs. (9) and (10) reflect the first half population (exploitation) and Eqs. (11)-(13) represent the other half population (exploration) as follows [40]:

For the exploitation-based population:

For $\frac{1}{3}Iter_{Max} < \text{iter} < \frac{2}{3}Iter_{Max}$

$$\overrightarrow{stepsize_i} = \overrightarrow{R_L} \otimes (\overrightarrow{Elite_i} - \overrightarrow{R_L} \otimes \overrightarrow{prey_i}) \quad (9)$$

where, $i = 1, 2, 3, \ldots n/2$

$$\overrightarrow{prey_i} = \overrightarrow{prey_i} + P.\overrightarrow{R} \otimes \overrightarrow{stepsize_i} \quad (10)$$

where $\overrightarrow{R_L}$ represents a vector of random numbers referring to the Lévy distribution.

For the exploration-based population:

$$\overrightarrow{stepsize_i} = \overrightarrow{R_B} \otimes (\overrightarrow{R_B} \otimes \overrightarrow{Elite_i} - \overrightarrow{prey_i}) \quad (11)$$

where, $i = n/2, \ldots n$

$$\overrightarrow{prey_i} = \overrightarrow{Elite_i} + P.CF \otimes \overrightarrow{stepsize_i} \quad (12)$$

$$CF = \left(1 - \frac{Iter}{Iter_{Max}} \right)^{\left(2 * \frac{Iter}{Iter_{Max}} \right)} \quad (13)$$

where, CF is a tuned parameter to control the step size of the predator.

3) THIRD PHASE: EXPLOITATION STAGE

In the final stage of the MPA, the predator moves more rapidly than the prey. In this rule, the mathematical model is adopted as shown [40]:

For $Iter > \frac{2}{3}Iter_{Max}$

$$\overrightarrow{stepsize_i} = \overrightarrow{R_L} \otimes (\overrightarrow{R_L} \otimes \overrightarrow{Elite_i} - \overrightarrow{Prey_i}) \quad (14)$$

where, $i = 1, 2, 3, \ldots n$

$$\overrightarrow{Prey_i} = \overrightarrow{Elite_i} + P.CF \otimes \overrightarrow{stepsize_i} \quad (15)$$

B. ESCAPING LOCAL MINIMA

In the marine life, eddy formation or Fish Aggregating Devices (FADs) influence the marine predator's behavior. Mathematically, the FADs are local minima. To prevent MPA from getting trapped in non-globally optima, Eq. (16) is applied [40].

$$\overrightarrow{Prey_i} = \begin{cases} \overrightarrow{Prey_i} + CF \left[\overrightarrow{y_{min}} + R \otimes \left(\overrightarrow{y_{max}} - \overrightarrow{y_{min}} \right) \right] \otimes \overrightarrow{U} \\ \quad \text{if } r \leq FAD \\ \overrightarrow{Prey_i} + [FAD \times (1 - r) + r] \left(\overrightarrow{Prey_{r1}} - \overrightarrow{Prey_{r2}} \right) \\ \quad \text{if } r > FAD \end{cases}$$

$$(16)$$

where $\overrightarrow{U}$ is a vector of zeros and ones, $\overrightarrow{y_{max}}$ and $\overrightarrow{y_{min}}$ are the vectors including upper and lower bounds of the dimensions,
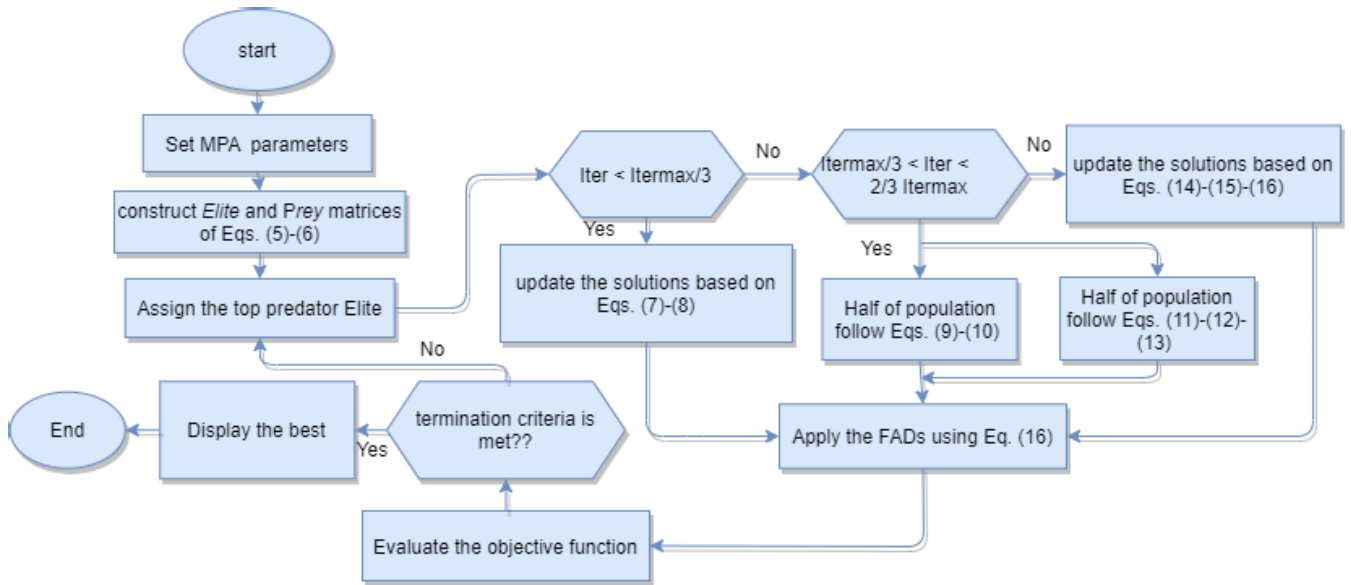
FIGURE 4. MPA optimization flowchart.

subscripts ($r1$ and $r2$) represent a random indices of *Prey* matrix. FAD usually is assigned a value of 0.2 [40].

The MPA is depicted in the flowchart of Fig. 4 to summarize the proposed algorithm structure [40]–[43].

IV. THE TEST SYSTEM: IEEE 48-BUS NETWORK

The MPA is applied to the IEEE-48 bus interconnected areas electrical power system grid [49]. This network consists of two interconnected regions as shown in Fig. 5. Prefix 1 identifies the elements of the first area, and prefix 2 identifies the elements in the second area. As an example, G 115 defines a unit of generation in the first area at bus number 15. Three transmission lines link the two areas with each other, and are marked in Fig. 5 as bold red lines. The system parameters are included in [49].

V. TUNING MPA PARAMETERS

This section investigates the impact of tuning three specific control parameters of the MPA performance as applied to the OPF problem. These parameters are (a) distribution of iteration between the three phases of the algorithm, (b) population of the second stage of the MPA, and (c) FAD's effect. As discussed in [40], these parameters govern the performance of the MPA.

A. IMPACT OF THE SHARE OF EACH PHASE IN NUMBER OF ITERATIONS

First, the strategy of one-third of iterations allocated to each phase is tested. Changing this ratio yielded slightly better results, as illustrated in Table 1. It can be concluded that the least cost for the OPF of the IEEE 48-Bus system could be obtained when the distribution of iterations is 3/5 for the first stage, 1/5 for the second stage and 1/5 for the third one.

TABLE 1. Variations in the distribution of iteration for each phase.

Distribution of iteration for each phase			Cost
1/3	1/3	1/3	86281.9
1/4	1/2	1/4	86281.9
1/2	1/4	1/4	86283.1
1/4	1/4	1/2	86283
1/5	3/5	1/5	86281.6
2/5	1/5	2/5	86282.5
1/5	2/5	2/5	86281.8
2/5	2/5	1/5	86282
3/5	**1/5**	**1/5**	**86281.5**
1/5	1/5	3/5	86281.9

B. IMPACT OF THE POPULATION OF THE SECOND STAGE

As stated earlier in Section III, the second stage of the MPA accomodates both exploration and exploitation, with the overall population split in half between these two steps. Table 2 shows the effect of changing the population distribution between exploration and exploitation on the quality of the OPF solution as applied to the IEEE 48 Bus system.

As seen from Table 2, the best result (minimum OPF cost) could be achieved when the distribution is divided into 2/3 for the prey and 1/3 for the predator.

C. IMPACT OF CHANGING THE FAD VALUE

As denoted in Section III, the FAD is imposed in the MPA to avoid getting trapped in local minima. In [40], FAD was set at 0.2. However, and as shown in Table 3, tuning the FAD to 0.3 instead can realize marginally better performance of the algorithm.

Based on the above, it can be concluded that – for the OPF of the IEEE-48 bus – tuning the following parameters of the MPA yields marginally better results:
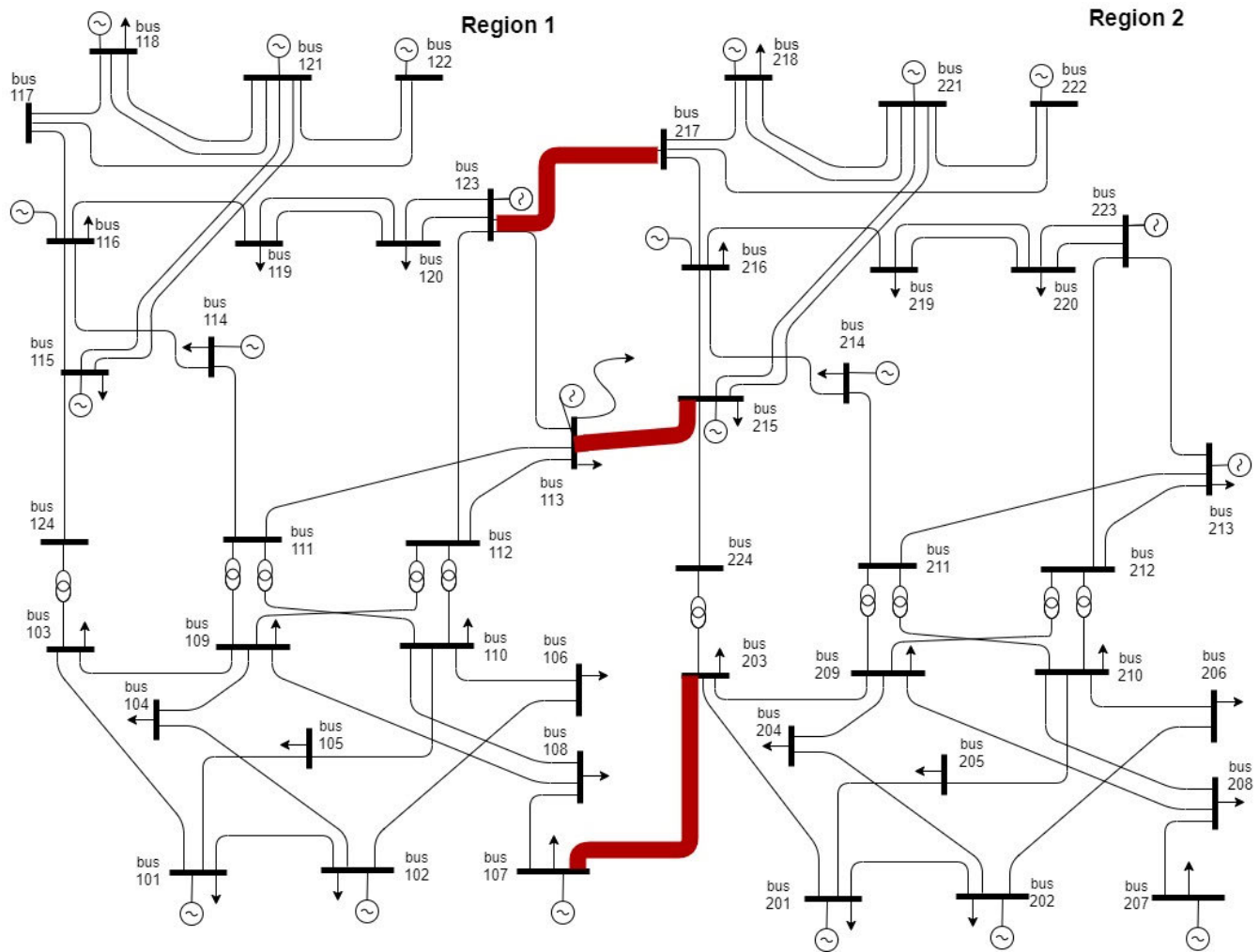
FIGURE 5. The IEEE-48 bus interconnected network.

TABLE 2. Variations in the population in the second stage.

Distribution of population in the second stage Prey Predator		Cost
1/2	1/2	86281.9
1/3	**2/3**	**86281.6**
2/3	**1/3**	**86281.6**
1/5	4/5	86282.1
2/5	3/5	86282.3
3/5	2/5	86281.7
4/5	1/5	86281.9

TABLE 3. Variations in the FAD.

FADs	Cost
0.2	86281.9
0.1	86282.7
0.3	**86281.6**
0.4	86282.1

OPF of the IEEE 48-Bus two-area system. Then, the effect of load and renewables variations on the MPA robustness is illustrated.

A. COMPARING MPA AND GA – NO INTERMITTENT RESOURCES

The OPF of the power system of Fig. 5 is calculated using both the tuned MPA and GA, without considering the impact of the renewables variability. Both OPF techniques explained in Section II are considered, namely:

- The holistic technique by considering the two connecting areas as one region.

- The distribution of iterations to: 3/5 for the first stage, 1/5 for the second stage and 1/5 for the third one.
- The population of the second stage to be distributed to 2/3 for the prey and 1/3 for the predator.
- FAD to be equal 0.3.

VI. COMPARING MPA AND GA

This section compares the performance of the tuned MPA against the well-established GA, as applied to solving the

TABLE 4. Optimum cost for OPF OF IEEE 48 bus two area system without renewables variability.

Cases under study	Initial cost =160286	
	GA	MPA
Holistic Approach	86352	86280
Inter-Bounded Approach	144394	144392
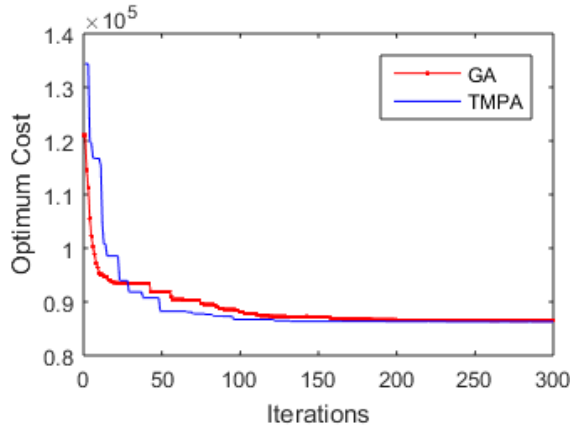
FIGURE 6. Convergence curve of the Holistic-based OPF without renewables variability.
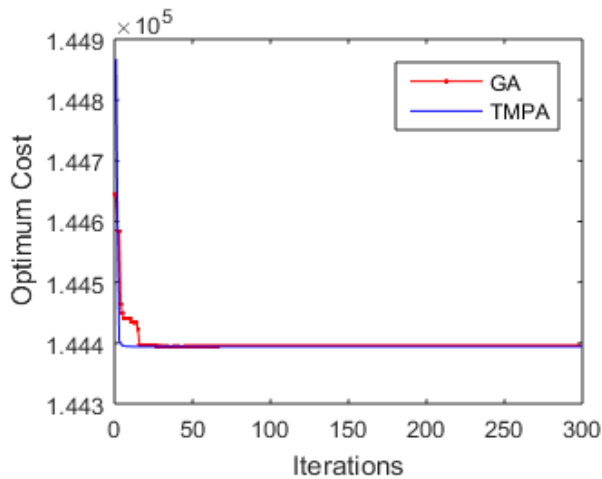
FIGURE 7. Convergence curve of the Inter-bounded OPF without renewables variability.

TABLE 5. Power flow results for the Holistic-based OPF without renewables variability.

Bus No.	Power Dem. (KW)	GA			MPA		
		Gen. Power (KW)	Volt	Angle (rad)	Gen. Power (KW)	Volt	Angle (rad)
101	108	62.66	1.01	-0.3457	62.4	1.05	-0.3279
102	97	62.68	0.99	-0.348	62.4	1.04	-0.3299
103	180	0	1.03	-0.2335	0	1.05	-0.2244
104	74	0	1.00	-0.3229	0	1.05	-0.3066
105	71	0	1.02	-0.3387	0	1.05	-0.3220
106	136	0	1.01	-0.3508	0	1.05	-0.3327
107	125	228.7	1.01	-0.2546	226.8	1.05	-0.2444
108	171	0	1.00	-0.3084	0	1.05	-0.2965
109	175	0	1.02	-0.2279	0	1.05	-0.2181
110	195	0	1.02	-0.2713	0	1.05	-0.2588
111	0	0	1.01	-0.108	0	1.05	-0.1032
112	0	0	1.04	-0.0872	0	1.05	-0.0837
113	265	515	1.00	0	516.9	1.00	0
114	194	0	0.97	-0.0578	0	1.05	-0.0551
115	317	66.8	0.97	0.0661	66.3	1.05	0.0567
116	100	155	0.98	0.0691	155	1.05	0.0582
117	0	0	0.98	0.1496	0	1.05	0.1287
118	333	400	1.02	0.1727	400	1.04	0.1498
119	181	0	1.02	0.0619	0	1.05	0.0536
120	128	0	0.98	0.0916	0	1.05	0.0821
121	0	400	0.97	0.1854	400	1.05	0.1609
122	0	300	1.01	0.296	300	1.05	0.2607
123	0	660	0.97	0.1233	660	1.05	0.1102
124	0	0	1.03	-0.0523	0	1.05	-0.0507
201	108	62.74	1.02	-0.3803	62.4	1.05	-0.3622
202	97	62.42	0.98	-0.3829	62.4	1.05	-0.3644
203	180	0	1.03	-0.2679	0	1.05	-0.2566
204	74	0	1.03	-0.3603	0	1.05	-0.3425
205	71	0	1.04	-0.3744	0	1.04	-0.3564
206	136	0	1.03	-0.3864	0	1.05	-0.3669
207	125	226.5	1.00	-0.2845	226.8	1.05	-0.2689
208	171	0	0.99	-0.3457	0	1.05	-0.3257
209	175	0	1.00	-0.2673	0	1.03	-0.2532
210	195	0	1.03	-0.3096	0	1.05	-0.2931
211	0	0	1.03	-0.146	0	1.05	-0.1393
212	0	0	0.98	-0.1247	0	1.05	-0.1198
213	265	516	0.96	-0.0382	517.3	1.05	-0.0429
214	194	0	1.02	-0.0933	0	1.05	-0.0918
215	317	66.51	0.99	0.0241	66.3	1.05	0.0190
216	100	155	1.02	0.029	155	1.05	0.0209
217	0	0	1.03	0.1056	0	0.96	0.0969
218	333	400	1.02	0.1266	400	1.05	0.1182
219	181	0	1.03	0.0268	0	1.05	0.0168
220	128	0	1.00	0.0596	0	1.05	0.0459
221	0	400	0.99	0.137	400	1.05	0.1278
222	0	300	0.97	0.2476	300	1.00	0.2388
223	0	660	0.99	0.092	660	1.05	0.0742
224	0	0	1.03	-0.0901	0	1.05	-0.0863

• The Inter-bounded technique, the algorithm is executed on each of the two areas separately, while considered the boundary conditions of the tie-lines between the two areas.

Table 4 illustrates the comparison between the optimum cost in each case. The corresponding values of the OPF variables are depicted in Table 5 and Table 6. The convergence rates of MPA and GA for both OPF approaches are shown in Fig. 6 and Fig. 7. In Fig. 8, the voltage profile curve is also presented for both inter-bounded and holistic approaches respectively.

From Table 4, the holistic (detailed) approach showed approximatly 54% reduction in cost compared to the initial solution. The inter bounded solution showed almost 10% reduction in the system operating cost.

It can be observed from the results of Table 4 that the tuned MPA outperformed the GA in terms of achieving better values for the OPF objective function, regardless of the OPF approach being used. Moreover, the curves of Fig. 6 and Fig. 7 shows that the MPA yielded faster convergences compared to the GA approach. These two findings indicate that the MPA is more accurate and faster than

TABLE 6. Power flow results of the interface busses for the inter-bounded OPF without renewables variability.

Bus No.	Power Dem. (KW)	GA			MPA		
		Gen. Power (KW)	Volt	Angle (rad)	Gen. Power (KW)	Volt	Angle (rad)
107	125	116.8	1.04	-0.2937	116.8	0.97	-0.299
113	265	258.5	1.00	0	258.6	1.00	0
123	0	660	0.95	0.1693	660	1.01	0.1634
203	180	0	1.04	-0.2511	0	0.96	-0.2557
215	317	66.3	0.97	0.0281	66.3	0.95	0.0297
217	0	0	0.99	0.119	0	1.05	0.1120

TABLE 7. Best locations of applied RERs for case 1.

Scenarios	GA		MPA	
	Location (bus)	Power (KW)	Location (bus)	Power (KW)
Wind RER	109	1710	223	1710
Solar RER	209	1710	215	1710
Wind and solar RERS	119	2280	204	2280

TABLE 8. Optimum cost with integration of RERs for case 1.

Generation sources	Cost	
	GA	MPA
Wind RER	82564.4	82262.4
Solar RER	82501	82235.8
Wind and solar RERS	80507.1	80223.3

the GA when applied to the OPF problems, regardless of the approach (holistic vs. inter-bounded). One more observation is with respect to comparing the convergence rates between Fig. 6 and Fig. 7 indicate that the inter-bounded approach yielded a much faster convergence rate than the hollistic approach, which is attributed to the assumption of decoupling the load flow solution of both regions in the inter-bounded approach.

Moreover, as can be seen in the results of Table 4, the hollistic approach yields significant reduction in the system operating cost compared to the inter-bounded approach. This can be attributed to the fact that the hollistic approach optimizes the voltages and flows across the entire interconnected power system, while the inter-bounded approach only optimizes the variables at the interface busses between different regions. This is also evident in the results of Fig. 8, where the voltages of almost all busses in both regions are changed and boosted to 1.05 pu to minimize reactive power flows (hence reducing system losses). On the other hand, the bus voltages with the inter-bounded approach are marginally changed (except for the interface busses). In addition, comparing the convergence rates of both approachs (Fig. 6 and 7) shows that the inter-bounded approach provides a fast optimization technique that mainly focus on changing the variables on few busses – namely the interface busses. This - of course - comes at the

TABLE 9. Detailed power flow with integration of wind RER only for case 1.

Bus No.	Power Dem. (KW)	GA			MPA		
		Gen. Power (KW)	Volt	Angle (rad)	Gen. Power (KW)	Volt	Angle (rad)
101	108	64.8	1.01	-0.3179	62.4	1.05	-0.3309
102	97	62.8	0.95	-0.3192	62.4	1.05	-0.3331
103	180	0	0.96	-0.2072	0	1.04	-0.2245
104	74	0	1.04	-0.2798	0	0.98	-0.3113
105	71	0	0.99	-0.3169	0	1.02	-0.3245
106	136	0	1.01	-0.3304	0	1.05	-0.3339
107	125	205	1.02	-0.2749	205.2	0.99	-0.2447
108	171	0	1.00	-0.3092	0	1.03	-0.2996
109	175	0	0.96	-0.171	0	1.04	-0.2179
110	195	0	1.03	-0.2546	0	1.05	-0.2592
111	0	0	0.98	-0.0865	0	1.05	-0.1013
112	0	0	1.00	-0.0682	0	1.03	-0.0808
113	265	438.8	1.00	0	423	1.00	0
114	194	0	0.98	-0.0343	0	1.05	-0.0497
115	317	66.3	1.00	0.0879	66.3	1.02	0.0638
116	100	155	1.03	0.0866	155	1.05	0.0667
117	0	0	0.96	0.1664	0	1.05	0.1386
118	333	400	0.98	0.1919	400	1.01	0.1610
119	181	0	0.97	0.0742	0	1.05	0.0640
120	128	0	0.99	0.1003	0	0.99	0.0960
121	0	400	0.96	0.2055	400	1.01	0.1733
122	0	298.7	1.01	0.3170	300	1.02	0.2777
123	0	660	1.00	0.1280	660	1.04	0.1271
124	0	0	0.96	-0.0218	0	1.05	-0.0475
201	108	62.7	0.96	-0.4399	62.4	1.05	-0.3211
202	97	63.28	0.96	-0.4429	62.4	1.05	-0.3228
203	180	0	0.99	-0.3121	0	1.05	-0.2272
204	74	0	1.04	-0.4232	0	1.04	-0.2998
205	71	0	1.00	-0.4361	0	0.99	-0.3130
206	136	0	1.04	-0.449	0	1.05	-0.3200
207	125	206.5	1.01	-0.3767	200	1.01	-0.2565
208	171	0	1.04	-0.4243	0	1.05	-0.2997
209	175	0	0.96	-0.3303	0	1.02	-0.2081
210	195	0	1.04	-0.3744	0	1.05	-0.2443
211	0	0	0.96	-0.2031	0	1.05	-0.0859
212	0	0	0.99	-0.1836	0	1.04	-0.0576
213	265	460.2	1.02	-0.1051	483.5	1.04	0.0186
214	194	0	0.97	-0.1389	0	1.04	-0.0388
215	317	67.16	0.99	-0.0013	66.3	1.05	0.0621
216	100	155	0.99	-0.0022	155	1.05	0.0740
217	0	0	0.96	0.0882	0	0.99	0.1397
218	333	399.3	1.02	0.1099	400	1.00	0.1613
219	181	0	1.05	-0.0144	0	1.05	0.0894
220	128	0	1.03	0.0088	0	1.05	0.1352
221	0	400	0.99	0.1202	400	1.04	0.1716
222	0	300	0.96	0.2392	300	1.03	0.2776
223	0	659.8	1.01	0.0341	660	1.05	0.1728
224	0	0	1.03	-0.1201	0	1.00	-0.0483

expense of a less optimal system cost compared to the holistic approach. As discussed in Section II-B, the inter-bounded approach can be used when different regions have different system operators, while a reliability coordinator takes care of the flows on the intertie lines.

B. EFFECT OF RENEWABLES VARIABILITY
After selection of the favorable tuning parameters for the executed technique (MPA), the effect of variable renewable sources (Wind and/or Solar) on the robustness of the MPA is investigated – as compared to the GA solver. Both cases – holistic and inter-bounded – are considered.

TABLE 10. Detailed power flow with integration of solar RER only for case 1.

Bus No.	Power Dem. (KW)	GA			MPA		
		Gen. Power (KW)	Volt	Angle (rad)	Gen. Power (KW)	Volt	Angle (rad)
101	108	62.6	0.98	-0.3708	62.4	1.00	-0.3412
102	97	63.13	0.95	-0.3731	62.4	1.05	-0.3433
103	180	0	0.98	-0.2548	0	1.05	-0.2350
104	74	0	1.04	-0.3486	0	1.03	-0.3195
105	71	0	0.99	-0.3637	0	1.05	-0.3345
106	136	0	1.01	-0.3743	0	1.05	-0.3451
107	125	204.6	1.01	-0.3166	215.4	1.05	-0.2781
108	171	0	0.98	-0.3596	0	1.05	-0.3208
109	175	0	0.96	-0.2523	0	1.05	-0.2291
110	195	0	1.01	-0.2941	0	1.05	-0.2707
111	0	0	0.96	-0.1189	0	1.03	-0.1099
112	0	0	1.04	-0.0976	0	1.05	-0.0906
113	265	591	1.00	0	585.2	1.00	0
114	194	0	0.96	-0.0691	0	1.05	-0.0628
115	317	68.3	1.03	0.0543	66.3	1.01	0.0488
116	100	155	0.99	0.0546	155	1.03	0.0512
117	0	0	0.97	0.1323	0	1.05	0.1241
118	333	400	1.01	0.1552	400	1.05	0.1457
119	181	0	1.05	0.0476	0	1.05	0.0453
120	128	0	0.99	0.0762	0	1.05	0.0728
121	0	400	1.01	0.1666	400	1.03	0.1574
122	0	300	0.96	0.2835	300	1.00	0.2640
123	0	660	0.99	0.1068	660	1.05	0.1004
124	0	0	1.01	-0.0598	0	1.05	-0.0619
201	108	62.7	0.96	-0.4641	62.4	1.02	-0.4127
202	97	63.35	0.96	-0.4665	62.4	1.05	-0.4147
203	180	0	0.96	-0.3327	0	0.99	-0.2996
204	74	0	0.98	-0.4382	0	1.05	-0.3907
205	71	0	1.00	-0.4607	0	1.05	-0.4071
206	136	0	1.03	-0.4733	0	1.05	-0.4181
207	125	210.2	0.98	-0.3916	211.6	1.05	-0.3377
208	171	0	0.98	-0.4428	0	1.05	-0.3861
209	175	0	1.05	-0.3393	0	1.05	-0.3014
210	195	0	0.97	-0.3925	0	1.04	-0.3441
211	0	0	1.02	-0.2157	0	1.05	-0.1858
212	0	0	1.00	-0.1983	0	1.05	-0.1695
213	265	467.3	1.05	-0.1216	472.2	1.05	-0.0968
214	194	0	0.98	-0.1527	0	1.04	-0.1275
215	317	67.15	1.00	-0.0127	66.3	1.05	-0.0027
216	100	155	0.99	-0.0144	155	1.05	-0.0042
217	0	0	0.97	0.0751	0	1.05	0.0740
218	333	400	1.02	0.0974	400	1.05	0.0943
219	181	0	0.98	-0.0267	0	1.05	-0.0145
220	128	0	0.96	0.0007	0	1.05	0.0092
221	0	400	0.96	0.1088	400	1.03	0.1047
222	0	300	0.98	0.2257	300	1.05	0.2062
223	0	660	0.95	0.0311	660	1.05	0.0346
224	0	0	1.01	-0.1323	0	1.00	-0.1120

TABLE 11. Detailed power flow with integration of both wind and solar RERs for case 1.

Bus No.	Power Dem. (KW)	GA			MPA		
		Gen. Power (KW)	Volt	Angle (rad)	Gen. Power (KW)	Volt	Angle (rad)
101	108	62.8	0.99	-0.3816	62.4	1.05	-0.3331
102	97	63.02	0.95	-0.3836	62.4	1.05	-0.3351
103	180	0	1.03	-0.268	0	1.05	-0.2302
104	74	0	1.03	-0.3528	0	1.05	-0.3120
105	71	0	0.99	-0.3779	0	1.05	-0.3271
106	136	0	1.01	-0.3909	0	1.05	-0.3377
107	125	196.7	1.02	-0.3346	194.8	1.05	-0.2665
108	171	0	1.02	-0.371	0	1.05	-0.3331
109	175	0	1.03	-0.2574	0	1.05	-0.2235
110	195	0	0.95	-0.3076	0	1.05	-0.2639
111	0	0	1.00	-0.1235	0	1.05	-0.1063
112	0	0	0.98	-0.1006	0	1.05	-0.0866
113	265	591	1.00	0	534.4	1.05	0
114	194	0	1.00	-0.0758	0	1.00	-0.0582
115	317	67.01	1.04	0.0421	66.3	1.05	0.0526
116	100	54.64	1.01	0.0433	155	1.05	0.0550
117	0	0	0.99	0.1195	0	1.05	0.1265
118	333	400	0.99	0.1424	400	1.05	0.1478
119	181	0	1.03	0.0582	0	1.00	0.0450
120	128	0	1.03	0.0823	0	1.05	0.0798
121	0	400	0.99	0.1545	400	1.01	0.1595
122	0	300	1.01	0.2639	300	1.05	0.2611
123	0	660	1.00	0.1091	660	1.05	0.1078
124	0	0	0.96	-0.0758	0	1.04	-0.0554
201	108	62.74	1.01	-0.4782	62.4	1.05	-0.3290
202	97	62.76	1.03	-0.4807	62.4	1.05	-0.3272
203	180	0	1.03	-0.3507	0	1.05	-0.2507
204	74	0	1.02	-0.456	0	1.05	-0.2533
205	71	0	0.97	-0.4773	0	1.05	-0.3365
206	136	0	1.03	-0.4896	0	1.05	-0.3537
207	125	194.2	0.96	-0.4266	196.2	1.05	-0.2967
208	171	0	0.97	-0.4721	0	1.05	-0.3364
209	175	0	1.01	-0.361	0	1.05	-0.2359
210	195	0	0.98	-0.4105	0	1.05	-0.2874
211	0	0	1.01	-0.2354	0	1.05	-0.1408
212	0	0	1.02	-0.2182	0	1.05	-0.1222
213	265	475.5	1.04	-0.1444	442.6	1.05	-0.0581
214	194	0	0.97	-0.1674	0	1.05	-0.0929
215	317	67.15	0.99	-0.0237	66.3	1.05	0.0179
216	100	155	1.02	-0.0286	155	1.05	0.0204
217	0	0	0.97	0.0608	0	1.05	0.0936
218	333	400	1.02	0.0823	400	1.03	0.1139
219	181	0	0.96	-0.0453	0	1.05	0.0143
220	128	0	0.96	-0.0215	0	1.05	0.0416
221	0	400	1.04	0.0922	400	1.05	0.1241
222	0	300	0.97	0.2058	300	1.05	0.2245
223	0	660	1.02	0.0049	660	1.05	0.0690
224	0	0	0.99	-0.1516	0	1.05	-0.0847

In each case three sensitivities are considered:

- Integration of wind generation only to cover 30% of demand.
- Integration of solar generation only to cover 30% of demand.
- Integration of both wind and solar generation to cover 40% of demand.

The algorithms will also select the best busses to connect the RERs to in order to minimize the overall system cost.

1) CASE 1: THE HOLISTIC TECHNIQUE

Table 7 depicts the best bus location and corresponding installed capacity RERs for each case in order to achieve the best solution under uncertainty in loads with MPA. The simulation results showed the suitable locations at which the RERS can be located. Table 8 shows the optimal costs corresponding to three sensitivity cases.

The corresponding values of the best control variables are shown briefly in Table 9, Table 10, and Table 11. Fig. 9, Fig. 10 and Fig. 11 show the convergence of the objective function in each case. It is shown that the optimal solution converged rapidly under different scenarios.
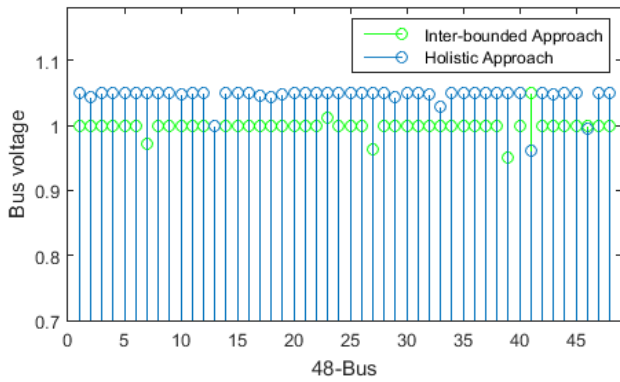
FIGURE 8. Voltage profile for the inter-bounded and holistic approaches without renewables variability.
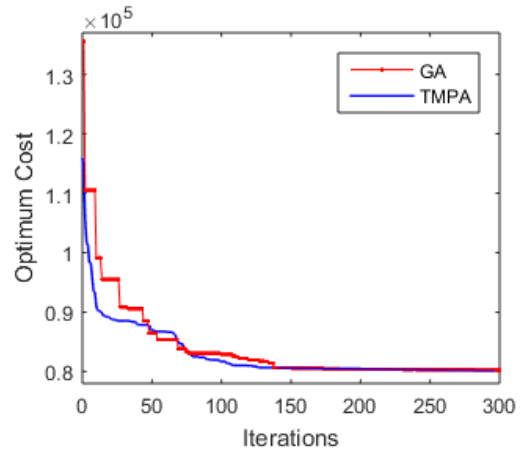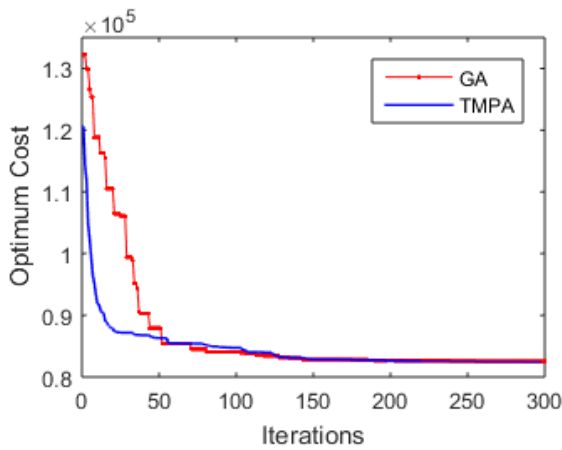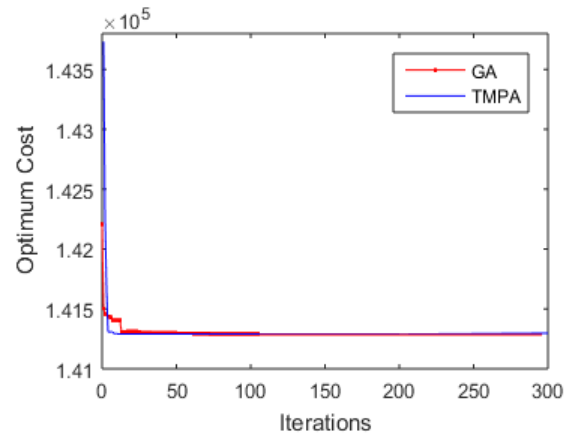

FIGURE 9. Convergence curve of MPA and GA with the integration of Wind RER only for case 1.
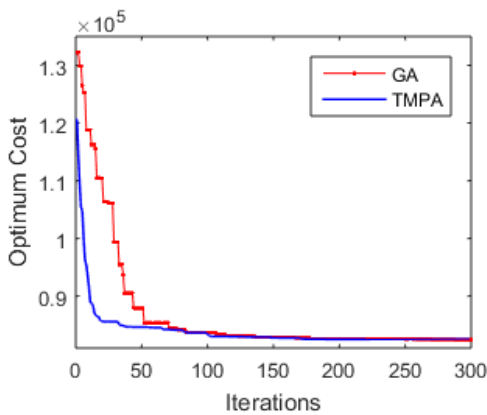

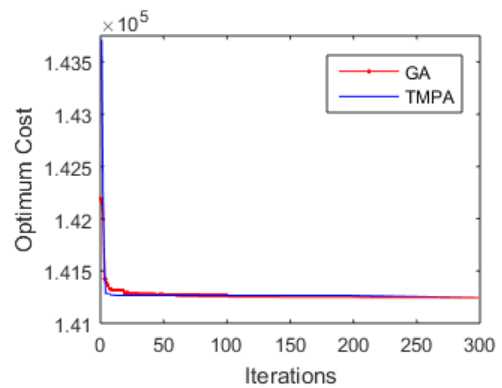**FIGURE 10.** Convergence curve of MPA and GA with the integration of Solar RER only for case 1.

FIGURE 11. Convergence curve of MPA and GA with the integration of Both Wind and Solar RERs for case 1.

FIGURE 12. Convergence curve of MPA and GA with the integration of Wind RER only for case 2.

FIGURE 13. Convergence curve of MPA and GA with the integration of Solar RER for case 2.

2) CASE 2: THE INTER-BOUNDED TECHNIQUE

In this case, the two interconnected areas are counted as one electric network and the integration of renewables by the three mentioned strategies are illustrated. Table 12 represents the best bus location as well as, the added power of RERs for each case in order to obtain the best solution uncertainty in loads with MPA. Table 13 outlines the optimal values of cost based on the three separate sensitivity cases mentioned before.
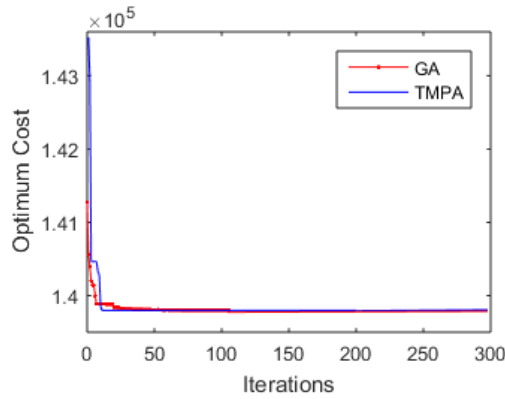
FIGURE 14. Convergence curve of MPA and GA with the integration of both Wind and Solar RERs for case 2.

TABLE 12. Best locations of applied RERs for case 2.

Scenarios	GA		MPA	
	Location (bus)	Power (KW)	Location (bus)	Power (KW)
Wind RER	113	1710	207	1710
Solar RER	121	1710	209	1710
Wind and solar RERS	104	2280	223	2280

TABLE 13. Optimum cost with integration of RERs for case 2.

Generation sources	Cost	
	GA	MPA
Wind RER	141291	141291
Solar RER	141267.3	141267.2
Wind and solar RERS	139798.9	139798.3

TABLE 14. Detailed power flow with integration of wind RERs for case 2.

Bus No.	Power Dem. (KW)	GA			MPA		
		Gen. Power (KW)	Volt	Angle (rad)	Gen. Power (KW)	Volt	Angle (rad)
107	125	75.14	1.00	-0.346	75	1.02	-0.278
113	265	207	1.00	0	207	1.00	0
123	0	660	0.96	0.164	660	0.95	0.1924
203	180	0	0.96	-0.275	0	1.03	-0.1624
215	317	66.3	1.02	0.021	66.3	0.99	0.0902
217	0	0	0.99	0.11	0	1.02	0.1792

TABLE 15. Detailed power flow with integration of solar RER for case 2.

Bus No.	Power Dem. (KW)	GA			MPA		
		Gen. Power (KW)	Volt	Angle (rad)	Gen. Power (KW)	Volt	Angle (rad)
107	125	75.18	1.01	-0.344	75	0.95	-0.3423
113	265	297	1.00	0	297	1.00	0
123	0	660	0.97	0.164	660	0.96	0.1639
203	180	0	0.96	-0.274	0	0.99	-0.2667
215	317	66.3	1.02	0.021	66.3	1.05	0.0232
217	0	0	1.00	0.11	0	1.05	0.1102

TABLE 16. Detailed power flow with integration of both wind and solar RERs for case 2.

Bus No.	Power Dem. (KW)	GA			MPA		
		Gen. Power (KW)	Volt	Angle (rad)	Gen. Power (KW)	Volt	Angle (rad)
107	125	75.08	1.05	-0.309	75	1.01	-0.3136
113	265	207	1.00	0	207	1.00	0
123	0	660	0.97	0.177	660	0.95	0.1852
203	180	0	1.04	-0.254	0	0.95	-0.2186
215	317	66.31	0.99	0.029	66.3	0.95	0.0728
217	0	0	1.03	0.119	0	1.05	0.1642

TABLE 17. Load profile for a week.

Day	Daily Peak Load (% of Weekly Peak)
Monday	93
Tuesday	100
Wednesday	98
Thursday	96
Friday	94
Saturday	77
Sunday	75

TABLE 18. Cost under different days.

Day	Cost	
	Holistic approach	Inter-bounded approach
Tuesday (100% load)	80223.3	139798.3
Sunday (75% load)	50037.2	125162.2

The values of the best control variables are illustrated briefly in Table 14, Table 15, and Table 16, based on case 2. To ensure the reliability of the MPA, the trials have been reiterated more than once. Fig. 12, Fig. 13 and Fig. 14 represent the convergence of the objective function in each case. It is shown that the optimal solution converged rapidly under different scenarios.

Albeit the results of Table 13 show that both MPA and GA yield similar accuracy, Figures 12, 13 and 14 indicate that the MPA converges faster, which indicates less computational burden compared to the GA.

Figure 15 shows the voltage profiles of the MPA with the integration of RERs based on cases 1 and 2 all the mentioned cases. It is noted that in case 1; holistic approach; the voltage is approximately 1.05 pu at many buses with the addition of RERs. While in case two; the inter-bounded approach; the voltage is approximately 1 pu at many buses with the addition of RERs. Similar to the discussion in Section IV-B, the inter-bounded approach yields a fast, yet less optimal solution, compared to the holistic approach. Depends on the need of
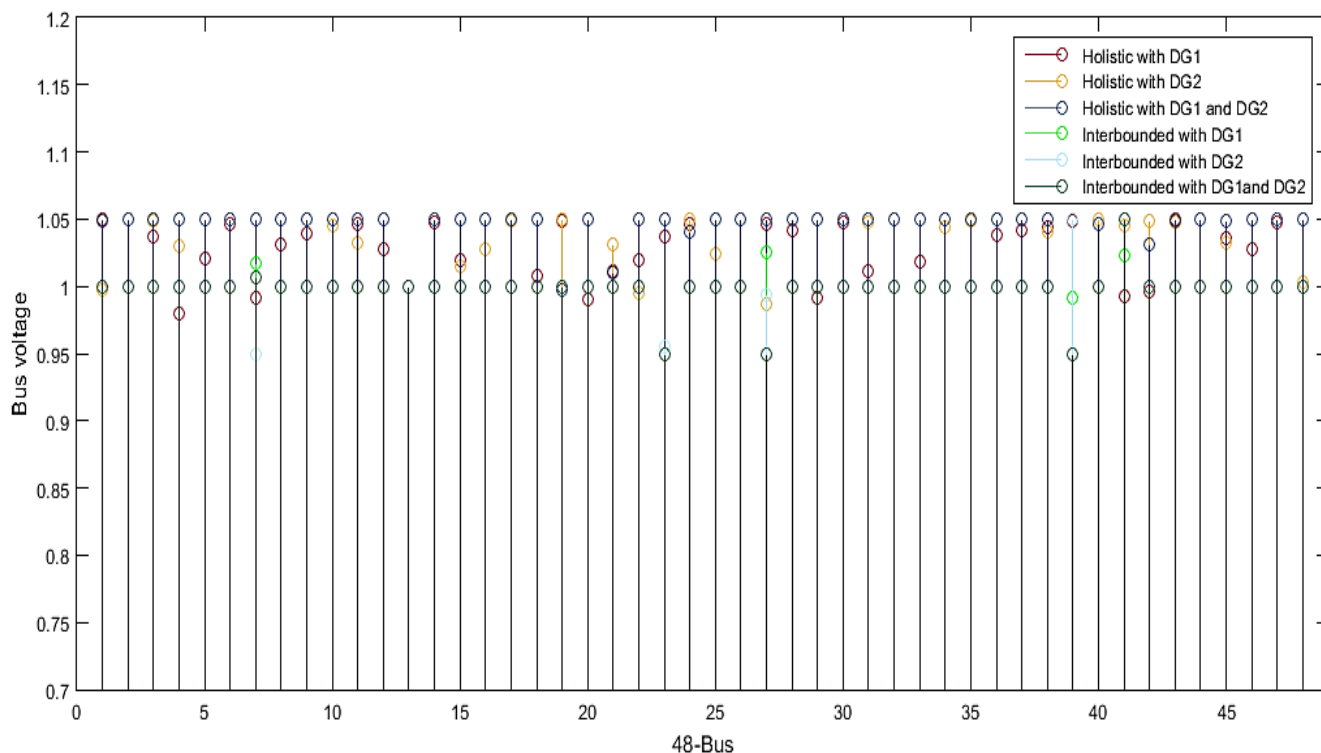
FIGURE 15. Voltage profile curves of MPA with integration of RERs for holistic and inter-bounded cases.

the system operator, both approachs are available for use. Howeber, in both cases the MPA marginally outperformed the GA in terms of solution accuracy (Tables 8 and 13). Moreover, the MPA superpassed the GA in terms of convergence rate (Figs. 9-14).

VII. WEEKLY LOAD PROFILE VARIABILITY
In this section, the weekly load profile resolution is firstly presented, and then the system is studied based on this load profile variability.

A. WEEKLY LOAD PROFILE
The weekday/weekend load profile shown in Table 17 [50] will be used to analyze the impact of load variability on the robustness of the MPA technique.

B. IMPACT OF LOAD VARIABILITY
The system is studied by MPA for a heavily loaded day (Tuesday) which is the peak day 100% load and light loaded day (Sunday) which is 75% load, considering both Solar and Wind RERs. The OPF costs are shown in Table 18.

The results of Table 18 show that the load reduction between the heavy loaded day (Tuesday) and light loaded day (Sunday) caused a significant reduction in the System cost. As discussed in Section VI, the holistic approach will always yield a far optimal solution compared to the inter-bounded approach, but needs much more computational

power. It is up to the system controller to choose the suitable approach based on the available computation resources and the urgency of an optimization decision.

VIII. CONCLUSION
A new innovative meta-heuristic MPA algorithm has been applied in this paper to solve the OPF problem in power systems, considering the variability of load and renewable generation. The optimum solver parameters were tuned for the MPA. Consequently, the performance of the MPA is compared with that of the well-known GA algorithm considering renewables and load variability. Two OPF models were used, namely holistic and inter-bounded models. The network considered in this paper is the two-connected areas, IEEE-48 electrical grid.

The results showed that while the holistic approach yields more optimal solution, it requires more computational power since it considers the entire interconnected system in the OPF model. On the other hand, the inter-bounded OPF approach yields much faster solution – yet less optimal compared to the holistic approach. The inter-bounded approach is suitable for fast decisions, and when the interties are operated by an independent reliability coordinator that only focuses on optimizing the tie line flows.

Regardless of the implemented OPF model, the results also indicated that the MPA outperforms the GA in terms of accuracy, computational burden, and convergence rates.

REFERENCES

[1] A. M. Ibrahim and R. A. Swief, "Comparison of modern heuristic algorithms for loss reduction in power distribution network equipped with renewable energy resources," *Ain Shams Eng. J.*, vol. 9, no. 4, pp. 3347–3358, Dec. 2018.

[2] S. Chandrasekaran, "Multiobjective optimal power flow using interior search algorithm: A case study on a real-time electrical network," *Comput. Intell.*, vol. 36, pp. 1–19, Mar. 2020.

[3] O. Herbadji, L. Slimani, and T. Bouktir, "Multi-objective optimal power flow considering the fuel cost, emission, voltage deviation and power losses using multi-objective dragonfly algorithm," in *Proc. Int. Conf. Recent Adv. Electr. Syst.*, Tunis, Tunisia, 2017, pp. 191–197.

[4] E. Kaymaz, S. Duman, and U. Guvenc, "Optimal power flow solution with stochastic wind power using the Lévy coyote optimization algorithm," *Neural Comput. Appl.*, pp. 1–30, Nov. 2020.

[5] W. Lu, M. Liu, S. Lin, and L. Li, "Fully decentralized optimal power flow of multi-area interconnected power systems based on distributed interior point method," *IEEE Trans. Power Syst.*, vol. 33, no. 1, pp. 901–910, Jan. 2018.

[6] N. M. Hassan, R. A. Swief, M. Z. Kamh, H. M. Hasanien, and A. Y. Abdelaziz, "Toward centralized/decentralized controlled power flow applying whale versus genetic optimization algorithms," *Int. J. Recent Tech. Eng.*, vol. 8, no. 4, pp. 1–8, Nov. 2019.

[7] T. A. Al-Muhawesh and I. S. Qamber, "The established mega watt linear programming-based optimal power flow model applied to the real power 56-bus system in eastern province of Saudi Arabia," *Energy*, vol. 33, no. 1, pp. 12–21, Jan. 2008.

[8] M. Pourakbari-Kasmaei and J. R. S. Mantovani, "Logically constrained optimal power flow: Solver-based mixed-integer nonlinear programming model," *Int. J. Electr. Power Energy Syst.*, vol. 97, pp. 240–249, Apr. 2018.

[9] A. A. Sousa, G. L. Torres, and C. A. Canizares, "Robust optimal power flow solution using trust region and interior-point methods," *IEEE Trans. Power Syst.*, vol. 26, no. 2, pp. 487–499, May 2011.

[10] P. Fortenbacher and T. Demiray, "Linear/quadratic programming-based optimal power flow using linear power flow and absolute loss approximations," *Int. J. Electr. Power Energy Syst.*, vol. 107, pp. 680–689, May 2019.

[11] G. Radman and J. Shultz, "A new derivation for Newton-based optimal power flow solution," *Electr. Power Compon. Syst.*, vol. 33, no. 6, pp. 673–684, Jun. 2005.

[12] X. Bai and H. Wei, "A semidefinite programming method with graph partitioning technique for optimal power flow problems," *Int. J. Electr. Power Energy Syst.*, vol. 33, no. 7, pp. 1309–1314, Sep. 2011.

[13] A. K. Laha, K. E. Bollinger, R. Billinton, and S. B. Dhar, "Modified form of Newton's method for faster load-flow solutions," *Proc. Inst. Elect. Eng.*, vol. 121, no. 8, pp. 849–853, Aug. 1974.

[14] J. F. Marley, D. K. Molzahn, and I. A. Hiskens, "Solving multiperiod OPF problems using an AC-QP algorithm initialized with an SOCP relaxation," *IEEE Trans. Power Syst.*, vol. 32, no. 5, pp. 3538–3548, Sep. 2017.

[15] A. Maffei, S. Srinivasan, P. Castillejo, J. F. Martinez, L. Iannelli, E. Bjerkan, and L. Glielmo, "A semantic-middleware-supported receding horizon optimal power flow in energy grids," *IEEE Trans. Ind. Informat.*, vol. 14, no. 1, pp. 35–46, Jan. 2018.

[16] S. Prakash, V. Rangta, N. S. Jayalakshmi, and V. K. Jadoun, "Optimal location of DGs in a distribution system for maintaining voltage profile and loss reduction using genetic algorithm," in *Proc. Int. Conf. Power Electron. IoT Appl. Renew. Energy Control (PARC)*. Mathura, India: GLA Univ., Feb. 2020, pp. 59–64.

[17] A. Y. Abdelaziz, F. M. Mohammed, S. F. Mekhamer, and M. A. L. Badr, "Distribution systems reconfiguration using a modified particle swarm optimization algorithm," *Electr. Power Syst. Res.*, vol. 79, no. 11, pp. 1521–1530, Nov. 2009.

[18] W. Bai, I. Eke, and K. Y. Lee, "An improved artificial bee colony optimization algorithm based on orthogonal learning for optimal power flow problem," *Control Eng. Pract.*, vol. 61, pp. 163–172, Apr. 2017.

[19] A. A. El-Fergany and H. M. Hasanien, "Single and multi-objective optimal power flow using grey wolf optimizer and differential evolution algorithms," *Electr. Power Compon. Syst.*, vol. 43, no. 13, pp. 1548–1559, Aug. 2015.

[20] F. P. Sakti, S. Sarjiya, and S. P. Hadi, "Optimal power flow using flower pollination algorithm: A case study of 500 kV java-bali power system," *Int. J. Inf. Technol. Electr. Eng.*, vol. 1, no. 2, pp. 45–50, Sep. 2017.

[21] H. Buch and I. N. Trivedi, "An efficient adaptive moth flame optimization algorithm for solving large-scale optimal power flow problem with POZ, multifuel and valve-point loading effect," *Iranian J. Sci. Technol., Trans. Electr. Eng.*, vol. 43, no. 4, pp. 1031–1051, Dec. 2019.

[22] Y. Y. Zakaria, R. A. Swief, N. H. El-Amary, and A. M. Ibrahim, "Optimal distributed generation allocation and sizing using genetic and ant colony algorithms," *J. Phys., Conf. Ser.*, vol. 1447, Jan. 2020, Art. no. 012023, doi: 10.1088/1742-6596/1447/1/012023.

[23] C. Shilaja and T. Arunprasath, "Optimal power flow using moth swarm algorithm with gravitational search algorithm considering wind power," *Future Gener. Comput. Syst.*, vol. 98, pp. 708–715, Sep. 2019.

[24] M. Soliman, A. Y. Abdelaziz, and R. M. El-Hassani, "Distribution power system reconfiguration using whale optimization algorithm," *Int. J. Appl. Power Eng.*, vol. 9, no. 1, pp. 48–57, Apr. 2020.

[25] N. M. Hassan, R. A. Swief, M. Z. Kamh, H. M. Hasanien, and A. Y. Abdelaziz, "Centralized/decentralized optimal load flow based on tuned whale optimization algorithm," in *Proc. Int. Conf. Innov. Trends Commun. Comput. Eng. (ITCE)*, Feb. 2020, pp. 352–358.

[26] H. Ouafa, S. Linda, and B. Tarek, "Multi-objective optimal power flow considering the fuel cost, emission, voltage deviation and power losses using multi-objective dragonfly algorithm," in *Proc. Int. Conf. Recent Adv. Elect. Syst.*, Tunis, Tunisia, 2017, pp. 1–7.

[27] A. K. Khamees, A. El-Rafei, N. M. Badra, and A. Y. Abdelaziz, "Solution of optimal power flow using evolutionary-based algorithms," *Int. J. Eng., Sci. Technol.*, vol. 9, no. 1, pp. 55–68, Apr. 2017.

[28] R. Swief, T. Abdel-Salam, and N. El-Amary, "Photovoltaic and wind turbine integration applying cuckoo search for probabilistic reliable optimal placement," *Energies*, vol. 11, no. 1, p. 139, Jan. 2018.

[29] W. Warid, H. Hizam, N. Mariun, and N. Abdul-Wahab, "Optimal power flow using the jaya algorithm," *Energies*, vol. 9, no. 9, p. 678, Aug. 2016.

[30] A. A. El-Fergany and H. M. Hasanien, "Tree-seed algorithm for solving optimal power flow problem in large-scale power systems incorporating validations and comparisons," *Appl. Soft Comput.*, vol. 64, pp. 307–316, Mar. 2018.

[31] A.-F. Attia, R. A. El Sehiemy, and H. M. Hasanien, "Optimal power flow solution in power systems using a novel sine-cosine algorithm," *Int. J. Electr. Power Energy Syst.*, vol. 99, pp. 331–343, Jul. 2018.

[32] T. L. Duong and T. T. Nguyen, "Application of sunflower optimization algorithm for solving the security constrained optimal power flow problem," *Eng., Technol. Appl. Sci. Res.*, vol. 10, no. 3, pp. 5700–5705, Jun. 2020.

[33] S. S. Reddy, "Optimal power flow with renewable energy resources including storage," *Electr. Eng.*, vol. 99, no. 2, pp. 685–695, Jun. 2017.

[34] U. Khaled, A. M. Eltamaly, and A. Beroual, "Optimal power flow using particle swarm optimization of renewable hybrid distributed generation," *Energies*, vol. 10, no. 7, p. 1013, Jul. 2017.

[35] D. Le Anh and D. Vo Ngoc, "Application of Cuckoo search algorithm for optimal power flow in power system," *GMSARN Int. J.*, vol. 9, pp. 45–50, Jun. 2015.

[36] S. S. Reddy, P. R. Bijwe, and A. R. Abhyankar, "Faster evolutionary algorithm based optimal power flow using incremental variables," *Int. J. Electr. Power Energy Syst.*, vol. 54, pp. 198–210, Jan. 2014.

[37] M. Ghasemi, S. Ghavidel, M. Gitizadeh, and E. Akbari, "An improved teaching–learning-based optimization algorithm using Lévy mutation strategy for non-smooth optimal power flow," *Int. J. Electr. Power Energy Syst.*, vol. 65, pp. 375–384, Feb. 2015.

[38] T. Niknam, M. R. Narimani, M. Jabbari, and A. R. Malekpour, "A modified shuffle frog leaping algorithm for multi-objective optimal power flow," *Energy*, vol. 36, no. 11, pp. 6420–6432, Nov. 2011.

[39] A. A. El-Fergany and M. H. Hasanien, "Salp swarm optimizer to solve optimal power flow comprising voltage stability analysis," *Neural Comput. Appl.*, pp. 1–17, Jan. 2019.

[40] A. Faramarzi, M. Heidarinejad, S. Mirjalili, and A. H. Gandomi, "Marine predators algorithm: A nature-inspired metaheuristic," *Expert Syst. Appl.*, vol. 152, Aug. 2020, Art. no. 113377.

[41] D. Yousri, T. S. Babu, E. Beshr, M. B. Eteiba, and D. Allam, "A robust strategy based on marine predators algorithm for large scale photovoltaic array reconfiguration to mitigate the partial shading effect on the performance of PV system," *IEEE Access*, vol. 8, pp. 112407–112426, 2020.

[42] M. A. Soliman, H. M. Hasanien, and A. Alkuhayli, "Marine predators algorithm for parameters identification of triple-diode photovoltaic models," *IEEE Access*, vol. 8, pp. 155832–155842, 2020.

[43] A. A. M. Al-Qaness, A. A. Ewees, H. Fan, L. Abualigah, and M. A. Elaziz, "Marine predators algorithm for forecasting confirmed cases of COVID-19 in Italy, USA, Iran and Korea," *Int. J. Environ. Res. Public Health*, vol. 17, pp. 1–14, Jan. 2020.

[44] M. A. M. Shaheen, H. M. Hasanien, S. F. Mekhamer, and H. E. A. Talaat, "Optimal power flow of power systems including distributed generation units using sunflower optimization algorithm," *IEEE Access*, vol. 7, pp. 109289–109300, Dec. 2019.

[45] M. G. Echeverri, J. M. L. Lezama, and J. R. S. Mantovani, "Decentralized AC power flow for multi-area power systems using a decomposition approach based on Lagrangian relaxation," *Revista Facultad Ingeniería Universidad Antioquia*, vol. 53, pp. 225–235, Jun. 2010.

[46] A. Y. Saber and G. K. Venayagamoorthy, "Efficient utilization of renewable energy sources by gridable vehicles in cyber-physical energy systems," *IEEE Syst. J.*, vol. 4, no. 3, pp. 285–294, Sep. 2010.

[47] A. Y. Saber and G. K. Venayagamoorthy, "Plug-in vehicles and renewable energy sources for cost and emission reductions," *IEEE Trans. Ind. Electron.*, vol. 58, no. 4, pp. 1229–1238, Apr. 2011.

[48] H. R. G. Ibrahim, "Impact of demand response and battery energy storage system on electricity markets," Ph.D. dissertation, Dept. Elect. Comput. Eng., Univ. Waterloo, Waterloo, ON, Canada, 2017.

[49] C. Grigg, P. Wong, P. Albrecht, R. Allan, M. Bhavaraju, R. Billinton, Q. Chen, C. Fong, S. Haddad, S. Kuruganty, W. Li, R. Mukerji, D. Patton, N. Rau, D. Reppen, A. Schneider, M. Shahidehpour, and C. Singh, "The IEEE reliability test system-1996. A report prepared by the reliability test system task force of the application of probability methods subcommittee," *IEEE Trans. Power Syst.*, vol. 14, no. 3, pp. 1010–1020, Aug. 1999.

[50] R. A. Swief, N. H. El-Amary, and M. Z. Kamh, "Optimal energy management integrating plug in hybrid vehicle under load and renewable uncertainties," *IEEE Access*, vol. 8, pp. 176895–176904, 2020.

HANY M. HASANIEN (Senior Member, IEEE) received the B.Sc., M.Sc., and Ph.D. degrees in electrical engineering from the Faculty of Engineering, Ain Shams University, Cairo, Egypt, in 1999, 2004, and 2007, respectively. From 2008 to 2011, he was a Joint Researcher with the Kitami Institute of Technology, Kitami, Japan. From 2012 to 2015, he was an Associate Professor with the College of Engineering, King Saud University, Riyadh, Saudi Arabia. He is currently a Professor with the Electrical Power and Machines Department, Faculty of Engineering, Ain Shams University. He has authored, coauthored, and edited three books in the field of electric machines and renewable energy. He has published more than 150 articles in international journals and conferences. His biography has been included in *Marquis Who's Who in the world* for its 28 edition, 2011. His research interests include modern control techniques, power systems dynamics and control, energy storage systems, renewable energy systems, and smart grid. He is an Editorial Board Member of *Electric Power Components and Systems* Journal. He was received the Encouraging Egypt Award for Engineering Sciences, in 2012, the Institutions Egypt Award for Invention and Innovation of Renewable Energy Systems Development, in 2014, and the Superiority Egypt Award for Engineering Sciences, in 2019. He is the IEEE PES Egypt Chapter Chair. He is a Subject Editor of *IET Renewable Power Generation, Ain Shams Engineering Journal and Electronics* (MDPI). He is the Editor-in-Chief of *Ain Shams Engineering Journal*.

ALMOATAZ YOUSSEF ABDELAZIZ (Senior Member, IEEE) received the B.Sc. and M.Sc. degrees in electrical engineering from Ain Shams University, Cairo, Egypt, in 1985 and 1990, respectively, and the Ph.D. degree in electrical engineering according to the channel system between Ain Shams University, Egypt, and Brunel University, U.K., in 1996. Since 2007, he has been a Professor of electrical power engineering with Ain Shams University. He has authored or coauthored more than 400 refereed journal articles and conference papers, 25 book chapters, and three edited books with Elsevier and Springer. He has supervised 80 master's and 35 Ph.D. theses. His research interests include the applications of artificial intelligence, evolutionary and heuristic optimization techniques to power system planning, operation, and control. He is also a member of IET and the Egyptian Sub-Committees of IEC and CIGRE'. He has been awarded many prizes for distinct researches and for international publishing from Ain Shams University and Future University in Egypt. He is the Chairman of the IEEE Education Society Chapter in Egypt. He is an Editor of *Electric Power Components and Systems* Journal. He is an editorial board member, an editor, an associate editor, and an editorial advisory board member for many international journals. He is currently seconded to the Future University as Professor.

RANIA A. SWIEF (Senior Member, IEEE) received the B.Sc. and M.Sc. degrees and the Ph.D. degree in deregulated market and price load market relations from Ain Shams University, Cairo, Egypt, in 1998, 2004, and 2010, respectively. She has contributed in many articles nationally and internationally. Since 2018, she has been an Associate Professor with the Electrical Power and Machine Department, Faculty of Engineering, Ain Shams University. She has many publications in local and international conferences. She has supervised many Ph.D. and master's degrees in the areas of smart grid, protection, deregulated market, and renewable energy. Her research interests include power system analysis, planning, and renewable energy.

MOHAMED Z. KAMH (Senior Member, IEEE) received the B.Sc. (Hons.) and M.Sc. degrees in electrical power and machines engineering from Ain Shams University, Cairo, Egypt, in 2003 and 2007, respectively, and the Ph.D. degree in electrical engineering from the University of Toronto, Toronto, ON, Canada, in 2011. He is currently an Assistant Professor with the Department of Electrical Power and Machines, Ain Shams University. He also works as the Technical Adviser of the Ministry of Electricity and Renewable Energy for Transmission Network Planning and Operation. He is a registered Professional Engineer in Egypt, as well as with the Provinces of Alberta and Ontario, Canada, where he worked for more than a decade as a utility leader in the fields of transmission system planning, operation, and engineering. His research interests include power system planning and operation, power electronics, distributed and renewable energy resources, smart grids, and application of artificial intelligence in the aforementioned fields.

NADA MAMDOUH HASSAN received the B.Sc. and M.Sc. degrees in electrical power and machines engineering from Ain Shams University, Cairo, Egypt, in 2011 and 2017, respectively. Her M.Sc. degree was in the area of renewable energy. She is currently a Teaching Assistant with the Department of Electrical Power and Machines, Higher Institute of Engineering and Technology-Fifth Settlement, Cairo. She has publications in international conference papers and journal articles. Her research interests include power system analysis, control, and renewable energy.

• • •